Evaluation on Mass Sensitivity of SAW Sensors for Different Piezoelectric Materials Using Finite Element Analysis

Amir Abdollahi, Zhongwei Jiang, Sayyed Alireza Arabshahi
Graduate School of Science and Engineering, Yamaguchi University,
2-16-1 Tokiwadai, Ube, Yamaguchi 755-8611, JAPAN

Abstract — The mass sensitivity of the piezoelectric surface acoustic wave (SAW) sensors is an important factor in the selection of the best gravimetric sensors for different applications. To determine this value without facing the practical problems and consuming long theoretical calculation time, we have shown that the mass sensitivity of SAW sensors can be calculated by a simple 3D finite element analysis (FEA) using ANSYS platform. The FEA data were used to calculate the wave propagation speed, surface particle displacements and wave energy distribution on different cuts of various piezoelectric materials. Meanwhile, to calculate more accurate results from FEA data, wave reflection problem was considered in the analysis. The results are used to provide a simple method for evaluation of their mass sensitivities.

I. Introduction

Surface acoustic wave (SAW) sensors are micro-electromechanical systems (MEMS) which are used for sensing small changes in the composition of the surface such as added mass by surface adsorption. The mass sensitivity for this type of sensors is the important criteria to select the appropriate sensor for desirable applications and precise measurements. To evaluate this value for different piezoelectric materials, some complex equations considering the wave propagation and energy distribution in the sensor substrate should be calculated [1]. In almost all the theoretical cases, one should consider some simplifications and analytical approaches to evaluate the different specifications of piezoelectric sensors e.g. the mass sensitivity [2]. Also these investigations for various piezoelectric materials can take considerable time due to the anisotropic construction of these materials. In the practical cases, difficulties and economical problems can restrict the investigation of various SAW sensors due to their micro sizes. Therefore some simple and primary simulations and analyses can be useful to investigate this type of sensors with various materials and substrate orientations especially before manufacturing and practical applications. One of the powerful methods to facilitate the investigation of the complex structures such as SAW sensors is the finite element (FE) numerical calculation. FE software can simulate various aspects of SAW devices concurrently and without considerable simplifications especially when the material of model has anisotropic properties and complex constitutive equations for wave propagation. In this paper, we present the simple and useful 3D FE analyses using ANSYS finite element software package to evaluate the mass sensitivity of surface acoustic wave sensors considering different piezoelectric materials. For the materials and orientations of the FE models, we applied the most commonly used cuts and piezoelectric materials which have been employed for the SAW sensors. Y-Z and Z-X cuts of lithium niobate ($LiNbO_3$) [3],[4], ST-X and ST-90°X cuts of quartz [5],[6], 36° Y-X cut of lithium tantalate ($LiTaO_3$) [7], and novel 22°Y-90°X cut of langasite (LGS) [8] are the materials for six sensors which were applied for our simulation. These cuts of materials have the good acoustic properties considering temperature coefficient of delay (TCD), electromechanical coupling coefficient (K^2) and the mass sensitivity. We provided two analyses to evaluate the mass sensitivities of these cuts as the SAW sensor. In the first analysis, the impulse response of each sensor was achieved and then the wave propagation speed or resonant frequency for the main mode was calculated. In the second analysis, after exciting the substrate with an oscillating signal, the wave energy and surface particle displacements were obtained from the FE analysis data considering the bulk wave reflection. The wave energy data were selected from the period when the bulk wave reflections do not deteriorate the energy value of the bulk elements. Using the appropriate data from two analyses accompanied with the analytical perturbation method formula [9], we calculated the mass sensitivity for each sensor.

II. Mass Loading

The simplest interaction, and the one most utilized for SAW sensor applications, is the response due to changes in the areal/mass density (mass/area) on the device surface. From the perturbation method theory [9], the general mass sensitivity formula which defines the decreasing change in resonant frequency is given by:

$$S = \frac{\Delta f}{\rho_s} = -\frac{f_0 \cdot \omega^2}{4}\left(\frac{u_x^2 + u_y^2 + u_z^2}{U}\right) \qquad (1)$$

where ρ_s is the surface mass density, ω is the operating angular frequency, f_0 is the mode resonant frequency, U is the average area density of the wave energy and u_x, u_y, and u_z are the SAW particle displacements at the surface of substrate. Also the dispersion law defines the relation between wave propagation speed (v_0) and resonant frequency (f_0) as below:

$$f_0 = v_0 / d \qquad (2)$$

where d is the periodicity of sensor.

For calculating the mass sensitivity, the values of f_0, U, u_x, u_y, and u_z should be derived from the piezoelectric coupled wave equations. FEA method can easily solve these complex equations and different values of phase velocity, wave energy and acoustic displacements can be obtained from FEA data. In the following sections after defining FE model, we

describe the procedure to obtain these data through two FEA analyses.

III. Finite Element Model

The finite element model of piezoelectric substrate has the dimensions of 490 μm propagation length, 420 μm width and 100 μm depth (Fig. 1). The dimensions of the structure were chosen to decrease the effects of acoustic reflection from the FE model boundaries, whilst also reducing the number of nodes required for simulation. The coupled-field element Solid5 was used for simulation. The dimension of the cubic surface element was chosen as 4.375 μm for each side. For the lower layers, we defined more 3 elements below each surface element with the same area but the height of elements increases with the spacing ratio of 16. Therefore the model was created such that the highest density of nodes was concentrated at the sensor surface to get more accurate data from the surface elements. The IDTs fingers were defined with a periodicity of 35 μm and aperture of 192.5 μm. The distance between input and output IDTs was considered as 96.25 μm. Also IDTs fingers were defined as mass-less conductors, represented as a set of nodes coupled by the voltage degree of freedom (DOF). For electrical boundary condition, the back surface of the model was electrically grounded to reduce the electromagnetic feed-through effect which is the interference of the electrical field between two transducers. For the mechanical boundary conditions, the FE model was mechanically fixed at only one node to satisfy the minimum static equilibrium condition. Fixing more nodes or the back surface of the model can increase the bulk wave reflection and making spurious data. This one node can be selected from any nodes except the surface and back nodes of the model. To define the cut and orientation of the FE model, the specific coordinate system as the crystal axes was adjusted to the mentioned cuts and orientations for each material.

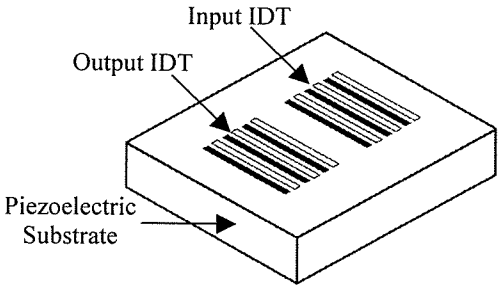

Fig. 1. Model of two ports SAW sensor.

IV. Finite Element Analyses

A. Analysis 1: Obtaining resonant frequency

In the first analysis, we performed the transient analysis for calculating the resonant frequency (f_0) for each sensor. First, we applied an impulse signal with the magnitude of 1V for the duration of 4 ns to one node of the input IDT and the simulation was run for 100 ns. To get an acceptable accuracy and to provide a conditional stability in the Newmark method the time step size (Δt) was considered as 0.5 ns. At the end of the analysis, the output voltage was recorded from one of the output IDT nodes and the frequency response of the sensor was obtained by FFT algorithm. The peak points of frequency responses indicate the main mode frequencies for SAW sensors and they are presented in Table I. The wave propagation speed can be obtained using equation (2). The last column of Table I represents the results of other researchers which are in a good agreement with our analysis results.

TABLE I
WAVE SPEED AND FREQUENCY FOR THE MOST COMMONLY USED MODE OF EACH SENSOR

Sensor	Resonant Frequency (MHz)	Wave Speed (m/s)	Reference Data (m/s)
22°Y-90°X LGS	83	2905	2944[8]
ST-X quartz	92	3220	3198[5]
Y-Z $LiNbO_3$	100	3500	3488[10]
36°Y-X $LiTaO_3$	121	4235	4220[7]
Z-X $LiNbO_3$	123	4305	4379[4]
ST-90X quartz	150	5250	5060[6]

B. Analysis 2: Calculating mass sensitivity

To calculate the mass sensitivity using equation (1), the values of wave energy (U) and the surface particle displacements (u_x, u_y, and u_z) should be acquired for each sensor. In this analysis, we used the FE model without defining the output IDT because the surface particle displacement and wave energy can be achieved from any surface nodes and bulk elements of the model respectively without defining any specific coupled nodes as the output IDT.Also the main important reason for defining the single input IDT for FE model is to remove the electromagnetic feed-through effect from the sensor responses specially for the materials with the low permittivity e.g. quartz and LGS. For the input IDT, the oscillating signal with the amplitude of 1V and obtained resonant frequency (f_0) in the first analysis was applied for each sensor. The time step size (Δt) and analysis duration were considered same as the first analysis. To acquire data after the simulation, the network of elements presented in Fig. 2(a) was considered. This network consists of one row of the surface elements, whose length (and thus quantity) are equal to the IDT aperture (44 elements), and the bulk [volumetric] elements beneath that surface. These elements are located one element farther than the last finger of the input IDT because from these near elements to the IDT, we could achieve more data in the shorter time of simulation and without the effect of surface wave reflection. In fact this elements network can be interpreted as the gate in the path of the acoustic wave to measure the wave energy. To calculate the mass sensitivity, the total kinematics energy for each column of the elements network (Fig. 2b) and the values of displacements (u_x, u_y, and u_z) for one surface node of each column were obtained from FEA elements energy and node displacements data respectively during the simulation. Also to compare the mass sensitivity

values, the operating angular frequency was assumed as $\omega = 200\pi$ rad/sec for all sensors in equation (1).

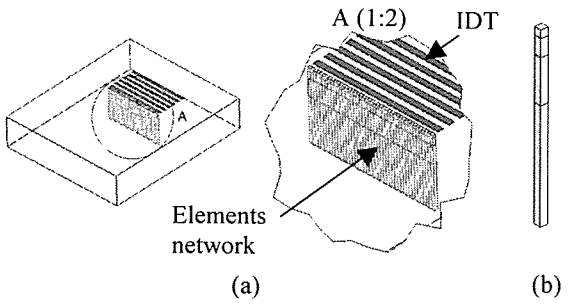

Fig. 2. (a) The network of elements selected from FE model (b) One column of network elements from the surface to the back side of FE model.

Using the mentioned data with equation (1) and dividing the total energy of the each column by the area of the surface element ($4.375 \times 4.375\ \mu m^2$) to acquire the area density of the wave energy (U), the mass sensitivity values were calculated for the elements network columns during the simulation. The sample mass sensitivity graph is presented for 36°Y-X cut of lithium tantalate in Fig. 3.

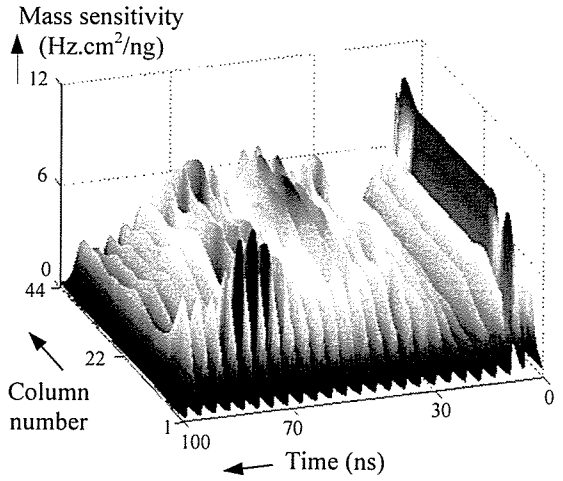

Fig. 3. Mass sensitivity graph for 36°Y-X $LiTaO_3$ SAW sensor.

As it is defined in equation (1), the wave energy should be considered as an average value. Therefore, the average value of the mass sensitivity graph can be obtained as the total mass sensitivity for each sensor. To calculate the average of the mass sensitivity graph, we should select the best period of the simulation without spurious data. The most important problem which can affect the FEA data in this analysis is the bulk wave reflection from the back surface of the sensor. It can especially deteriorate the bulk element energy data and then it causes the spurious values in the mass sensitivity graph. Therefore the effect of this reflection should be evaluated for each sensor .For this purpose one of the lowest elements (longest element) of the elements network was considered and the energy value for this element was obtained during the simulation. The sample graph of this value for 36°Y-X $LiTaO_3$ is presented in Fig. 4.

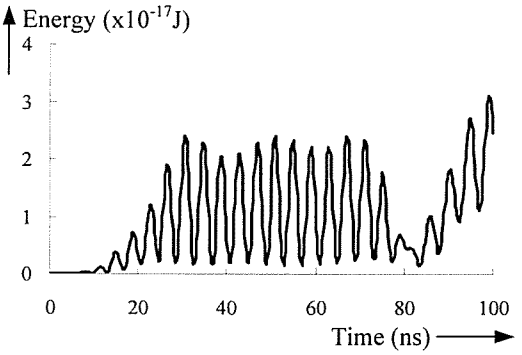

Fig. 4. Energy of the lowest element for 36°Y-X $LiTaO_3$ SAW sensor.

Considering Fig. 4, the bulk energy distribution can be evaluated for 36°Y-X $LiTaO_3$. The distribution procedure consists of four distinguishable periods. First period is the gradual increasing of energy amplitude due to the propagation of bulk wave from the surface source of energy (IDT signal).This initial distribution of energy lasts until the bulk acoustic waves distribute completely in the sensor substrate and the bulk acoustic waves reach the stable condition. This period starts from the beginning of the simulation until about 30 ns in Fig. 4. After this period, the wave energy amplitude almost becomes stable until the bulk waves reflection interferes considerably with incident waves. This interference can be detected from any significant energy decrease in the energy graph. The stable period is between about 30 ns to about 70 ns in Fig. 4. The small decreases of the energy amplitude in this period are due to the weak reflection of bulk waves. After the stable period, reflected bulk waves start to beat the incident waves. This beating actually occurs when unsynchronized reflected waves damped the incident wave energy and it causes the gradual decrease of energy to a minimum value. This value indicates that the incident and reflected waves are in the most unsynchronized condition and it is the end of beating period. This period can be detected between 70 ns to 83 ns in Fig. 4. The last period is the period when the bulk and reflected waves gradually become synchronized, therefore the energy value increases significantly with this synchronization as it is obvious in Fig. 4 between 83 ns to the end of the simulation. This final period lasts until a maximum energy value which is reached with the next beating period. These four periods can be usually detected in any SAW sensors with the period lengths and starting times depend on the substrate material, orientation and the type of reflected waves. We evaluated the bulk energy graphs for the mentioned six sensors and then we detected the stable period for each sensor same as we did for 36°Y-X $LiTaO_3$ in Fig. 4.Then we used the mass sensitivity graph to calculate the average value of mass sensitivity in the stable period. Table II presents this value and the stable period for each mentioned sensors. Also other researchers' results for mass sensitivity of these sensors are presented in this table to show the validation of our analysis.

TABLE II
MASS SENSITIVITIES AND STABLE PERIODS FOR SAW SENSORS

Sensor	Mass Sensitivity ($Hz.cm^2/ng$)	Stable Period (ns)	Reference Data ($Hz.cm^2/ng$)
22°Y-90°X langasite	14	15 – 25	-
ST-X quartz	13.5	15 – 30	13.4[11]
Y-Z $LiNbO_3$	7	25 – 35	7.4[3]
Z-X $LiNbO_3$	4	25 – 40	4[12]
36° Y-X $LiTaO_3$	2.5	30 – 70	2.9[13]
ST-90X quartz	2.5	30 – 40	1.6[14]

According to Table II, the most mass sensitive SAW sensor is the novel 22°Y-90°X cut of langasite following by conventional ST-X quartz gravimetric sensor. The novel 22°Y-90°X cut of langasite first introduced and identified with shallow penetration depth by Berkenpas et. al.[8]. The important point in Table II is that for high mass sensitive sensors, the stable periods start faster than low mass sensitive ones. This relationship verifies logically our results since the high mass sensitivity represents weak penetration and short travel distance of wave energy to the bulk of the sensor and acoustic waves reach the stable condition faster. The starting time of stable period for 22°Y-90°X langasite and ST-X quartz sensors is about 15 ns whilst this time for 36° Y-X $LiTaO_3$ and ST-90X quartz with low mass sensitivities is about 30 ns. Another point is that lower wave propagation speed usually causes the higher mass sensitivity. This fact is obvious for sensors with the considerable difference in wave propagation speeds (Tables I and II). Table I shows that the novel 22°Y-90°X cut of langasite has the lowest wave propagation speed as the most mass sensitive sensor.

V. CONCLUSION

Two FEM analyses were introduced to evaluate the mass sensitivity for six types of SAW sensors with different piezoelectric materials. In the first analysis, the impulse response of each sensor was achieved using two IDTs FE model and exciting impulse signal. Then from the impulse response, the main resonant frequency was detected as the exciting frequency. Using this frequency in the second analysis to stimulate the single IDT FE model with the oscillating signal, the values of surface displacements and element energies were obtained to calculate the mass sensitivity value through perturbation equation. Results showed that 22°Y-90°X langasite SAW sensor is the most mass sensitive sensor following by conventional Rayleigh ST-X quartz SAW sensor.

REFERENCES

[1] B. A. Auld, *Acoustic Fields and Waves in Solids.* New York: Wiley, 1973, vol. 1.

[2] S. W. Wenzel and R. M. White, "Analytic comparison of the sensitivities of bulk-wave, surface-wave, and flexural plate-wave ultrasonic gravimetric sensors," *Appl. Phys. Lett.* , vol. 54, No. 20, pp. 1976-1978, May 1989.

[3] J. Enderlein, E. Chilla and H. J. Frohlich, "Comparison of the mass sensitivity of Love and Rayleigh waves in a three-layer system," *Sensors and Actuators A*, vol. 41, pp. 472-475, 1994.

[4] Y. Jin and S. G. Joshi, "Propagation of a quasi-shear horizontal acoustic wave in Z-X lithium niobate plates," *IEEE Trans. on Ultrason., Ferroelec., and Freq. Control*, vol. 43, No. 3, pp. 491-494, May 1996.

[5] S. Wu, L. Wu, J. H. Chang, F. C. Chang, "SAW modes on ST-X quartz with an AlN layer," *Material Letters*, vol. 51, pp. 331-335, November 2001.

[6] K. Kalantar Zadeh, A. Trinchi, W. Wlodarski, A. Holland, "A novel Love-mode device based on a ZnO/ST-cut quartz crystal structure for sensing applications," *Sensors and Actuators A*, vol. 100 pp. 135-143, 2002.

[7] D. A. Powell, K. Klanatar-zadeh, W. Wlodarski, "Numerical calculation of SAW sensitivity: application to $ZnO/LiTaO_3$ transducers," *Sensors and Actuators A*, vol. 115, pp. 456-461, July 2004.

[8] E. Berkenpas, S. Bitla, P. Millard, and M. P. Cunha, "Pure Shear Horizontal SAW Biosensor on Langasite," *IEEE Trans. on Ultrason., Ferroelec. , and Freq. Control*, vol. 51, No. 11, pp. 1404-1411, November 2004.

[9] Z. Wang, J. D. N. Cheeke, C. K. Jen, "Perturbation Method for Analyzing Mass Sensitivity of Planar Multilayer Acoustic Sensors," *IEEE Trans. on Ultrason., Ferroelec., and Freq. Control*, vol. 43, No. 5,pp. 844-851, September 1996.

[10] B. Draft, "Acoustic Wave Technology Sensors," *IEEE Trans. on Microwave Theory and Techniques*, vol. 49, No. 4, pp. 795-802, April 2001.

[11] A. J. Ricco and S. J. Martin, "Multiple-frequency SAW devices for chemical sensing and materials characterization," *Sensors and Actuators B*, vol. 10, pp. 123-131, 1993.

[12] F. Josse, J. C. Andle, J. F. Vetelino, R. Dahint, and M. Grunze, "Theoretical and experimental study of mass sensitivity of PSAW-APMs on ZX-$LiNbO_3$", *IEEE Trans. on Ultrason., Ferroelec., and Freq. Control*, vol. 42, No. 4, pp. 517-524, July 1995.

[13] F. Josse, F. Bender, and R. W. Cernosek, "Guided Shear Horizontal Acoustic Wave Sensors for Chemical and Biochemical Detection in Liquids", *Anal. Chem.*, vol. 73, pp. 5937-5944, 2001.

[14] J. A. Ogilvy, "The mass-loading sensitivity of acoustic Love wave biosensors in air", *J. Phys. D: Appl. Phys.*, vol. 30, pp. 2497-2501, April 1997.